Bioaerosol Transport and Sensor in Passenger Aircraft

Carlos Miguel Loureiro dos Santos Simões Raposo

carlos.s.raposo@tecnico.ulisboa.pt

Instituto Superior Técnico, Lisboa, Portugal

October 2022

Abstract

To aid the prevention and mitigation of the next pandemic, aircraft cabins must be continuously designed to ventilate effectively any contaminant dispersed in the air, and eventually allowing the early detection of an event of pathogen spreading using bioaerosol sensors. A RANS simulation, employing a modified k-ε approach and involving a detailed diffuser geometry, was used to accurately simulate the complex behavior of the ventilation jets and compare the results obtained with available experimental data. The modified realizable k-ε model was validated using quantitative and qualitative methods for a half-row cabin.

Subsequently, a contaminant was continuously injected into the center and side of the 3-row cabin, and ultimately conjugated with the use of gaspers. Briefly, it was found that, if gaspers are normal to the wall, the conjugated effect with the moist air flow vortex and thermal plume creates a condition of still air, thereby promoting diffusion and decreasing dispersion. Finally, either with gaspers turned on or off, the suggested locations for future sensors would be on the ceiling right above the passenger, and in the backseat surface of the front seat.

Keywords: aircraft cabin; contaminant dispersion; HVAC; RANS simulation; bioaerosols.

1. Introduction

In the year of 2019, the world was hit with the COVID-19 pandemic caused by a coronavirus, later confirmed to be transmissible via aerosols. According to Our World in Data, by October of 2022 there were already 6.56 million of deaths and 624 million of cases. Multiple measures that affected the world were taken like lockdowns, social distancing, mask use, air travel restrictions which had an impact on the world economy and people's physical and psychological states.

The aviation industry was affected by these measures by having an overall reduction of 50% of seats in 2020 and 40% in 2021. In terms of gross passenger operating revenues, there was a loss of 372 billion dollars in 2020 and 324 billion dollars in 2021 [1]. There was a joint effort by the industry and regulators to earn the public trust and several studies and presentations were published [2]. In particular, USTRANSCOM published a report with high quality experimental data done in real airframes that could be used to further improve numerical simulation and its validation. However, the essential data to accurately simulate aircraft remains confidential like the geometry of the diffusers and the air conditions, which are essential because they will define the airflow behavior. This could lead to major limitations and errors in studies of independent researchers creating a gap between the manufacturers and independent researchers either from academia or institutions. In part, this is a safe measure to prevent leaking to public media conclusions that could alarm people unnecessarily, but transparency of data is the key to continue research.

The objective of thesis [3] is to find suitable locations for bioaerosol sensors inside the aircraft cabin of commercial flight which would allow an early warning about possible infected passengers and, ultimately, contributing to improve the control of various respiratory pathogens spread by air travel. Therefore, first it was needed to study the airflow behavior using real diffuser geometry, secondly compare with available experimental data, thirdly study contaminants behavior and finally, the locations with higher concentrations would be candidates for bioaerosol sensors.

To help continue research to be closer to the real aircraft, this study focused on studying the mockup of Boeing 767 in Kansas State University reported to have salvaged diffusers and stating all the steps and assumptions throughout the 3D modeling and choice of turbulence model. The files of the used 3D model will be made available at ResearchGate and researchers are welcome to use and modify them.

2. Background

Due to COVID pandemic, there have been recent studies addressing this topic. Aiming to determine exposure risk, using optical sensors and collection techniques, dispersion and deposition of tracer aerosols was tested in the airframes of Boeing 767 and 777, on ground and in flight conditions, with gaspers active on ground [4], in a complementary investigation to a previous report [5]. These experimental results were compared in a computational study for a Boeing 737 where a manikin coughed polydisperse aerosols [6]. Both studies came to the conclusion that there is a low exposure risk.

In order to be able to compare data with the airframe testing, there is a need to accurately model the airflow. There are several mock-up cabins available worldwide, organized in [3]. The KSU mock-up cabin can be used to directly compare because it has real salvaged parts of the diffuser from Boeing 767. A summarized review of studies of ACER laboratory can be found in [7]. Mahmoud [8] studied experimentally aerosol dispersion using tracer gas in several situations, i.e. continuous injection point source, and a coughing manikin, both with ISOPass deployed and undeployed, in the B737 mockup, the B767 mockup and the same B767 mockup using a different ventilation system more alike to airbus cabins.

Only few computational studies modeled a more detailed diffuser. Lin et al. [9] [10] reported that RANS simulations significantly underpredicted the turbulence intensity, therefore, using LES and experimental results they tuned a modification to a RANS k-ε model with the goal of increasing the accuracy of the RANS simulation. They demonstrated that the turbulent kinetic energy was approximately eight times larger in LES than using standard k-ε modeling. Mazumdar [11] modeled the entire KSU-767 cabin with the RNG k-ε approach and compared with experimental data; it was reported that the diffuser breaks the main jet from the tubes into smaller jets that are governed by the spacer buttons and wall connectors locations, however there was a negligible net longitudinal flow with strong local longitudinal flows [3].

The KSU-767 cabin is composed of ducting, diffuser, storage bin and seats. Before the air arrives to the cabin it passes through a HVAC air filter, blown to desiccant dehumidification wheels and then an air conditioning system composed of three loops, subsequently proceeding to an electric heater, and finally arriving to the cabin ductwork. The cabin is composed of 11 rows with seats following the layout of the economy section (2-3-2) of a Boeing 767-300 aircraft, with the mixed class configuration type A door (24 first class seats and 224 economy seats) [12] [13]. The seats in the mock-up are filled with manikins wrapped with electric wire to create a thermal output of 100W. For the contaminant study, the injector is made of a copper tube with 25.4 mm diameter. Gaspers were installed in 2012 in rows 5, 6 and 7 [14];they are kept at a pressure of 498.18 Pa providing a flow rate of 1.6 L/s when fully opened; each gasper centerline or Personal Air Outlet (PAO) is separated 3 in (76.2 mm) from each other. The air from the gasper is extracted from the main supply duct.

3. Implementation

3.1 3D Modeling

Aiming to accurately model the KSU-767 cabin, extensive analysis of the documentation by KSU authors were analyzed [15] [8]. Extensive details and drawings of the geometry used in this study can be found in [3]. The reference frame is always the same, in the figures a cube with the axes is indicative of the view at that figure.

The diffuser slot gap, i.e., the area between the edge of the radius of the stowage bin and the tip of the diffuser at the ceiling, is assumed to be the sum of the radius of the storage bin 0.75 in with the gap between the tip of diffuser and the end of the storage bin 0.5 in, summing to 1.25 in (31.75 mm). The spacing from the cabin centerline to the diffusers tip is 6.625 in (168.275 mm). Further details of the dimensions are in [7].

3.2 Computational Methods

The computational study was divided into different stages to accomplish the goal of the present investigation. In the first stage, the computational domain was defined as half the row 6 and used to verify the performance of turbulence models as well as to define parameters to build a good quality mesh. In the second stage, the computational domain was set as the west portion of rows 5,6 and 7. In the third stage, the computational domain was redefined as the west and east portion of rows 5,6 and 7. Finally, in the fourth stage, gaspers were added to the domain. This study will only focus on steady state conditions. In the second and

third stages, the turbulence model was chosen to be the modified realizable *k-ε* approach, and the Eulerian transport of species was used to simulate a continuous injection of a mixture of He and CO_2 in steady state conditions with moist air. In the fourth stage, gaspers were added at every row with moist air, and the flow conditions at the inlet nozzle were updated to account for the loss of volumetric flow rate. For the 2nd, 3rd and 4th stages, the applied turbulence model was the RANS modified realizable *k-ε* (rkε-mod).

3.3 Computational Domain

To build the 3D model of the cabin, SolidWorks 2020 was used and then converted to Parasolid format. To clean the geometry of the 3D model and define the surfaces to be boundary conditions Ansys SpaceClaim 2021 was used. To handle the meshing, Ansys Fluent 2021 R1 was used for meshing and simulation. [16]

The cabin geometry includes the internal parts of the diffusers (spacer buttons, connectors, joint spacers) which account for many walls and small features in small portion of the domain. This creates difficulties in creating a good quality mesh, possibly enhancing wall effects from the turbulence models. However, this is necessary to accurately model the flow that passes through the slot.

The longitudinal length of the full cabin of 11 rows is the same as the length of the west diffuser section 377.1 in (9.57834 m). The maximum transversal length of the cabin is 186 in (4.7244 m) and the height of the diffuser tip is 1.9812 m, while the maximum height is 82.5 in (2.0955 m). When choosing the geometry to simulate, only the seats and manikins from the desired row are kept. The manikins are modeled as simple box shaped based on previous literature [17]. Gaspers were modeled as simple cylinders directed normal to the surface they were in; the diameter and velocity were computed using relations from the literature [18].

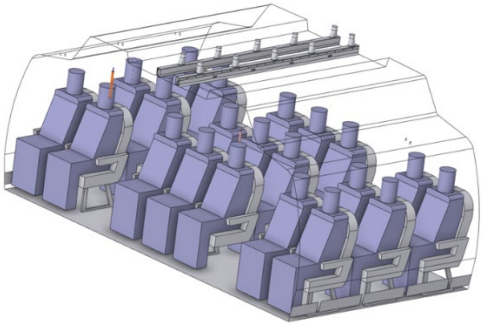

Figure 1. 3D view of 3-rows cabin domain

The reference frame of the domain was the same as referenced in KSU documents. The origin is at the intersection between the cabin floor, the symmetry plane and the south wall, making *z* positive from south wall to north wall, *y* positive from the floor to the ceiling, and *x* positive when it is at the west portion and negative when is at east portion.

Figure 1 shows the domain used in the 3rd and final stages. The geometry was extracted using the extracting volume tool from Spaceclaim. To avoid generation of mesh failure, a CAD correction was made: the spacing buttons were extruded until the next metal sheet, the manikins shoulder area was pulled to avoid merging the face with the seats.

3.4 Turbulence Modeling

In previous work [9] [11] this kind of geometry was simulated using a modified *k-ε* model and a standard RNG *k-ε* model employing standard wall functions. The Finite Volume Method is used for the discretization of the flow equations. The Reynolds Averaging of the Navier Stokes (RANS) equations can be found in Fluent's manual [16].

The chosen turbulence model is a modified version of the realizable *k-ε* model, by changing the source term S_k in the turbulent kinetic energy *k*-equation and changing the turbulence Prandtl number for the turbulent dissipation rate σ_ε, based on findings from the literature [9]. Equations (1) and (2) presented here are the original realizable *k-ε* model implemented in Fluent for the transport of turbulent kinetic energy (k), and its dissipation rate (ε) respectively.

$$\frac{\partial}{\partial t}(\rho k) + \frac{\partial}{\partial x_j}(\rho k u_j) = \frac{\partial}{\partial x_j}\left[\left(\mu + \frac{\mu_t}{\sigma_k}\right)\frac{\partial k}{\partial x_j}\right] + G_k + G_b - Y_M + S_k - \rho\varepsilon \quad (1)$$

$$\frac{\partial}{\partial t}(\rho \varepsilon) + \frac{\partial}{\partial x_j}(\rho \varepsilon u_j) = \frac{\partial}{\partial x_j}\left[\left(\mu + \frac{\mu_t}{\sigma_\varepsilon}\right)\frac{\partial \varepsilon}{\partial x_j}\right] + C_{1\varepsilon}\frac{\varepsilon}{k}(C_{3\varepsilon}G_b) - C_2\,\rho\frac{\varepsilon^2}{k+\sqrt{\nu\varepsilon}} + S_\varepsilon + \rho C_1 S\varepsilon \quad (2)$$

The default constants are $C_{1\varepsilon} = 1.44$; $C_2 = 1.9$, $\sigma_k = 1.0$, $\sigma_\varepsilon = 1.2$. In the realizable model, C_μ is a function of the mean strain S and rotation rates $\tilde{\Omega}_{ij}$, angular velocity of system rotation and turbulence fields k and ε. C_μ recovers standard value of 0.09 for an inertial sublayer in an equilibrium boundary layer. The option to include the rotational term $-2\varepsilon_{ijk}\omega_k$ was enabled.

To implement the turbulence model modification, source terms of the *k*-equation used in Fluent were compared with the one used in the literature to integrate the previous applied constant in [9] $C_{k2} = 0.77$, a new constant had to be created $C_{k3} = 1 - 0.77 = 0.23$ and integrated in the User Defined Function (UDF) as

shown in equation (3). The term $(S_k - \rho\varepsilon)$ is from equation (1) while the term $(C_{k2}\rho\varepsilon)$ arises from the k-equation in [9].

$$\begin{cases} S_k = C_{k3}\rho\varepsilon \\ S_k - \rho\varepsilon = C_{k2}\rho\varepsilon \end{cases} \rightarrow C_{k3} = 0.23 \quad (3)$$

The turbulence Prandtl number for the turbulence dissipation rate was directly implemented in the dialog box as $\sigma_\varepsilon = 1.67$. Near-wall modeling was handled with Menter-Lechner functions to provide y^+ insensitive wall treatment.

3.5 Contaminants Modeling

For the species transport, the Eulerian approach was chosen. The conservation equation of a species i is treated using the transport of mass fraction of each species Y_i in eq. (4).

$$\frac{\partial}{\partial t}(\rho Y_i) + \nabla \cdot (\rho \vec{u} Y_i) = -\nabla \cdot \vec{J}_i + R_i + S_i \quad (4)$$

$$X_i = Y_i \frac{M_m}{M_i} = \frac{Y_i}{M_i}\left(\frac{\rho RT}{p}\right) \quad (5)$$

The options of Diffusion Energy Source and Thermal diffusion options were enabled. Nitrogen was defined as the last species in the species dialog box of Ansys Fluent. Mole fraction X_i is related to mass fraction Y_i using molecular weights of the species M_i and mixture M_m in eq. (5).

3.6 Materials and operating conditions

When the flow was simulated without species, the material that was considered was dry air. When species were turned on, there were 6 different species: nitrogen N_2, oxygen O_2, water vapor H_2O, argon Ar, carbon dioxide CO_2 and helium He. In Fluent, the materials were defined using the ideal gas law and kinetic theory. The operating conditions are the same for every simulation. The Boussinesq's temperature was chosen to be 21°C because at steady state conditions the average temperature is known to be between 21°C and 22.5°C. The operating pressure was the same as inside the mock-up, set to 98882.53193 Pa, and the gravity acceleration -9.79958 m/s^2 on the y-direction [19].

3.7 Solution Methods

For the single-phase simulations, the coupled method with default pseudo transient explicit relaxation factors was used for the pressure-velocity coupling and changed to the Semi-Implicit Method for Pressure Linked Equations-Consistent (SIMPLEC) when species transport was activated. The discretization of pressure was used with the Pressure Staggering Option (PRESTO!). The discretization of gradient used the least squares cell based approach and the rest of the variables used second order upwind.

Residuals were also monitored. For the single-phase, continuity residuals were kept below 1×10^{-2}, for velocities under 1×10^{-5}, for turbulent kinetic energy and dissipation rate under 1×10^{-5}, and for energy under 1×10^{-7}. For the species simulation, residuals of He and CO_2 were kept below 1×10^{-5}, and for Ar, H_2O and O_2 below 1×10^{-7}. To ensure convergence, multiple physical quantities were monitored.

3.8 Mesh Generation

The mesh was composed of prism layers and polyhedral elements. Special care was taken in the region of $1 < y^+ < 5$, so a local face size was chosen near the small parts of the diffuser (0.2 mm in the buttons). The surface mesh was set to have a minimum of 0.5 mm and maximum of 50 mm. The generated volume mesh had 2.51 million elements with a minimum orthogonal quality of 0.122 and a maximum aspect ratio of 508. The high aspect ratio cells are formed on the areas with a high face size and a small prism layer height. This was a compromise to not increase more the number of elements. It is noted that the diffuser region ($y > 1.9812$ m), i.e., above the slot, contains 89% of the total number of cells. The final volume mesh for the half 6th row can be seen in Figure 2, while Figure 3 shows the details around the slot.

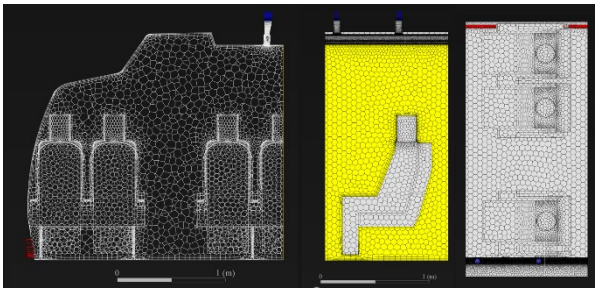

Figure 2. Volume mesh for the west portion of 6th row.

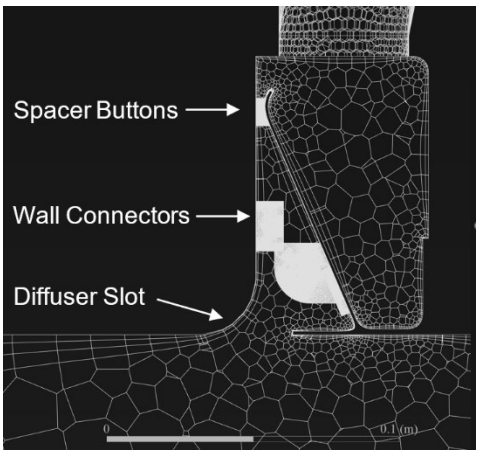

Figure 3. Zoom-in of the mesh near the diffuser slot.

A mesh with similar parameters was generated for the 3 rows with injectors and gaspers. Smaller local face sizes were defined at the injector and gasper faces when

the domain simulated changed. The domain for 3 rows with both sides without gaspers contained 5.78M elements, and with gaspers it was formed by 6.51M elements.

3.9 Boundary Conditions

As mentioned earlier, our goal was to simulate the same conditions as those in the mock-up of KSU. The inlets were the supply nozzles that feed the diffuser, with a diameter of 60.325 mm, with a flow rate of 1400 CFM (660.73 L/s) distributed through 34 nozzles. This defines an average inlet velocity to be 6.799 m/s and at a static temperature of 15.6 °C. The outlets were allowed to have reverse flow and prescribed at a temperature of 22°C. To better simulate the physical behavior of the flow, translational Periodic Boundary Conditions (PBC) were defined at the front and back faces of the domain with flow defined for the z axis, with a pressure gradient of 0 Pa/m and 21°C for the backflow. When just the west portion of the domain was simulated, a symmetry condition was applied to the plane $x = 0$. The manikins were set to heat flux of 52.82 W/m^2. When gaspers were added, the flow rate directed to the supply nozzles was adjusted. There are 21 gaspers, totaling 33.6 L/s, thus, 627.13 L/s are directed to the 34 nozzles giving an average inlet velocity of 6.453 m/s. Geometrically, the gaspers were assumed to be the same as in [18], therefore the same empirical relations could be used to determine the equivalent cylinder diameter (6) and average velocity (7).

$$d_{gasper} = \frac{4QB}{\pi B^*} \tag{6}$$

$$U_{m,0} = \frac{\pi}{4Q}\left(\frac{B^*}{B}\right)^2 \tag{7}$$

By considering $B = 6.2$, $B^* = 0.75$ m^2/s and applying the volumetric flow rate Q =1.6 L/s used in KSU, the equivalent diameter d_{gasper} results 16.84mm, and the average velocity at the circular face $U_{m,0}$ is 7.183 m/s. Physically there is just one injector at the simulated cabin domain, therefore, after convergence, the profiles of velocity, temperature, turbulent kinetic energy and turbulent dissipation rate were extracted and applied at the front and back faces. This way, it was possible to specify the species molar fraction to be the same as the supply nozzle. In the case of gaspers, a trade-off was taken to not simulate more rows, as this would be true for an infinite number of rows; however, the mock-up in KSU has only gaspers at rows 5, 6 and 7.

When the species were simulated, the molar fractions of moist air with a relative humidity (RH) assumed to be 15% were prescribed at the inlets of the supply nozzles. The supply air CO_2-concentration read by instruments was 400 ppm, so the applied molar fraction (X_i) at the inlets of CO_2 was set to 400 ppm as well. ($X_{CO2,moist\ air} = 0.04\%$) . The injector of the contaminant was a mixture of CO_2 (Q_{CO2} = 5L/min) and He (Q_{He}=3.07L/min). The injector speed had an average velocity of 0.2654 m/s and a temperature of 15.6 °C. For reference, the universal gas constant used was R_u = 8.314472 J/(kg·K). The rest of the properties were computed using ideal gas mixtures properties and relations [20]. As for the turbulence parameters, the turbulence intensity (TI) was calculated using equation (8) for fully developed duct flow and the Reynolds number was computed using the diameter (9) [21].

$$TI = 0.16\, Re_{Dh}^{-1/8} \tag{8}$$

$$\mathrm{Re}_{D_h} = \frac{\rho U D_h}{\mu} \tag{9}$$

$$TI = \frac{1}{|U|}\sqrt{\frac{2}{3}k} \tag{10}$$

4. Results

4.1 Half-row Air Simulation

During the first stage of the numerical simulations, several categories of turbulence models were experimented. In summary, turbulence models employing the k-ε approach performed the best overall, k-ω and SST models performed poorly in the region past the slot. The 3-equation model k-kL-ω performed qualitatively well, however, when checked in quantitative comparisons with experimental results from the probe it exhibited spikes of velocity without physical meaning.

Before applying the modification to the turbulence model, it was noticed that this modification was computed in isothermal conditions for a supply nozzle flow rate about 60% of the flow rate set in KSU-767 supply nozzle (0.6Q_{KSU} =11.2 L/s , Q_{KSU} =19.4 L/s). Therefore, a validation of the turbulence model was needed to advance to the next phase. To accomplish this important task, the contours of velocity were compared with for different conditions: isothermal flow with 60% of the flow rate, non-isothermal flow with 60% of the flow rate, and non-isothermal flow with 100% of the flow rate. The Coanda effect at the non-isothermal condition [22] was clearly decreased by the thermal plumes from the manikins which resulted in directing the jet more to the center of the side passengers. Hence, the flow was divided into two main vortices in the transversal plane (XY-plane). This is due to strong buoyancy effects from the thermal plumes of the manikins. The isothermal results were consistent with Lin 2005 [9].

It is well known that k-ε models are dissipative and the present modification allowed to decrease the dissipation. So, the surface averaged turbulent kinetic energy at the slot area was monitored. It was found that for the realizable k-ε non-modified model $TI_{slot} = 41\%$ and $k_{slot} = 0.93$ m^2/s^2, while for the modified model, $TI_{slot} = 66\%$ and $k_{slot} = 1.9$ m^2/s^2. As for the 3-equations transition model k-kL-ω, it was found that the flow is highly transitional, and the total fluctuating kinetic energy at the slot area was $k_{slot} = 3.8$ m^2/s^2

Quantitative experimental data of velocity magnitude obtained by an omnidirectional TSI Inc. probe near the slot [23] was compared with results from the simulation. In Figure 4, the velocity from the computational probe with different turbulence models is overlayed with the experimental data, and the west diffuser geometry is scaled to the z-direction.

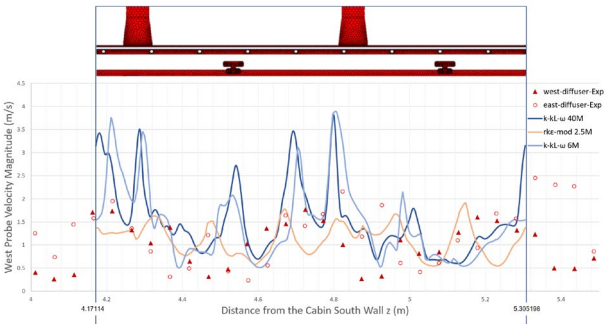

Figure 4. Velocity magnitude at west probe.

In the slot area, the flow was rather complex as reported in the literature. In Figure 5, one may observe the plots of turbulent kinetic energy, velocity magnitude, turbulence intensity and static temperature at the slot. The data in the plot of turbulence intensity is computed using equation (10).

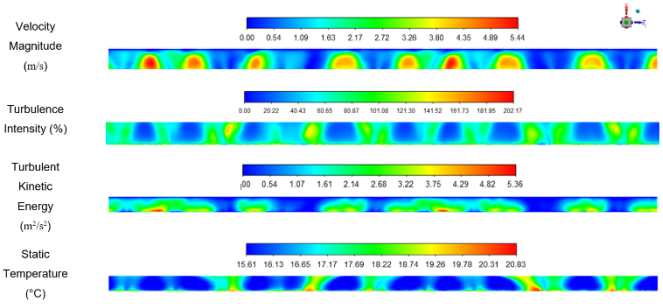

Figure 5. Contours of flow quantities at the slot area.

4.2 Three-rows Simulation

In Figure 6 it can be seen the results of the simulation from 3 rows when the injection at G6 was activated with species model. Despite the geometrical asymmetry in the diffuser parts, i.e., the diffuser buttons, connectors and joints not being in the same plane and the seats not being on the same plane, the flow appears to be symmetric. It is noted that in this domain, the spacer joints were not simulated. The domain could be halved, however, to simulate the injection at the center of the cabin D6, the west and east portion needed both to be simulated.

Furthermore in Figure 6, there is a significant longitudinal velocity on the aisles area and the flow is governed by two large vortices in the transverse plane. In the symmetry plane, the influence of the thermal plume makes the velocities reach 38 cm/s. The injector inlet has a velocity of 26 cm/s, however, globally the gas does not significantly disturb the flow, therefore one may assume that it behaves mostly as a tracer gas or passive contaminant. Regarding the temperatures, when 3 rows are simulated with the injector turned on G6, the average temperature of the cabin is 22.3°C, while the average temperature of the manikins is 32.1°C.

4.3 Contaminants

The full 11-row cabin interior with the origin of the reference frame and numbers of rows and letters of columns can be seen in Figure 7. Gaspers are considered to be 533 mm in front of the seat headrest, hence the gaspers on the 5th row are located at $z = 3.63855$ m, on the 6th row at $z = 4.47853$ m, and on the 7th row at $z = 5.31343$ m [14]. The first gasper of the 2-cluster on rows F, G correspond to $x = 1.82762$m, and the second has $x = 1.89938$m.

Figure 7 shows the results of the molar fraction of CO_2 in ppm overlapped with the experimental data from the literature [8] at the plane of breathing area y=1.25m. The injector center face at D6 is at (x, y, z) = (0.005465 m, 1.250235 m, 4.621249 m), while the injector center face at G6 is at (x, y, z) = (2.06414 m, 1.250234 m, 4.61185 m). The distances of the points in the same line are 0.84 m between each other, and the experimental results are overlayed in the pictures. Discrepancies to the experimental results are noticeable. This difference can be explained by the absence of gaspers in the simulation which would create high momentum cold jets and decrease the momentum of the thermal plume as well as, depending on the direction of gaspers, redirect the trajectory of the contaminants.

Furthermore, one limitation of this simulation is to imply periodic boundary conditions which would create an infinite number of rows; however, the mock-up cabin is composed of only 11 rows. According to the image of the trajectory of the tracer gas suggested by Shehadi [24], this would create one large vortex near each end and two vortices near the center, probably caused by the influence of the physical cabin walls at the extremities.

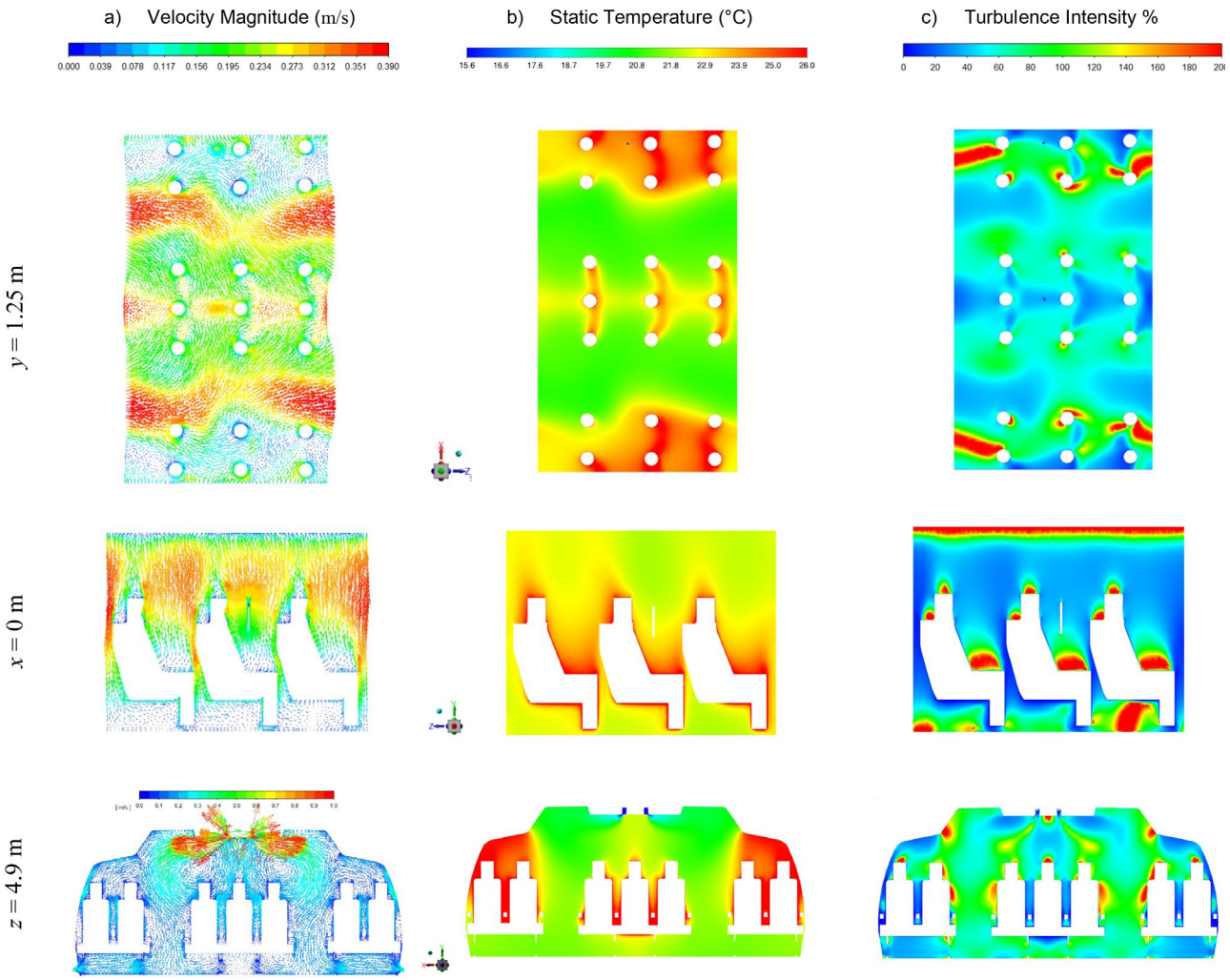

Figure 6. Velocity, temperature, and turbulence intensity contours for 3 rows with G6 injector.

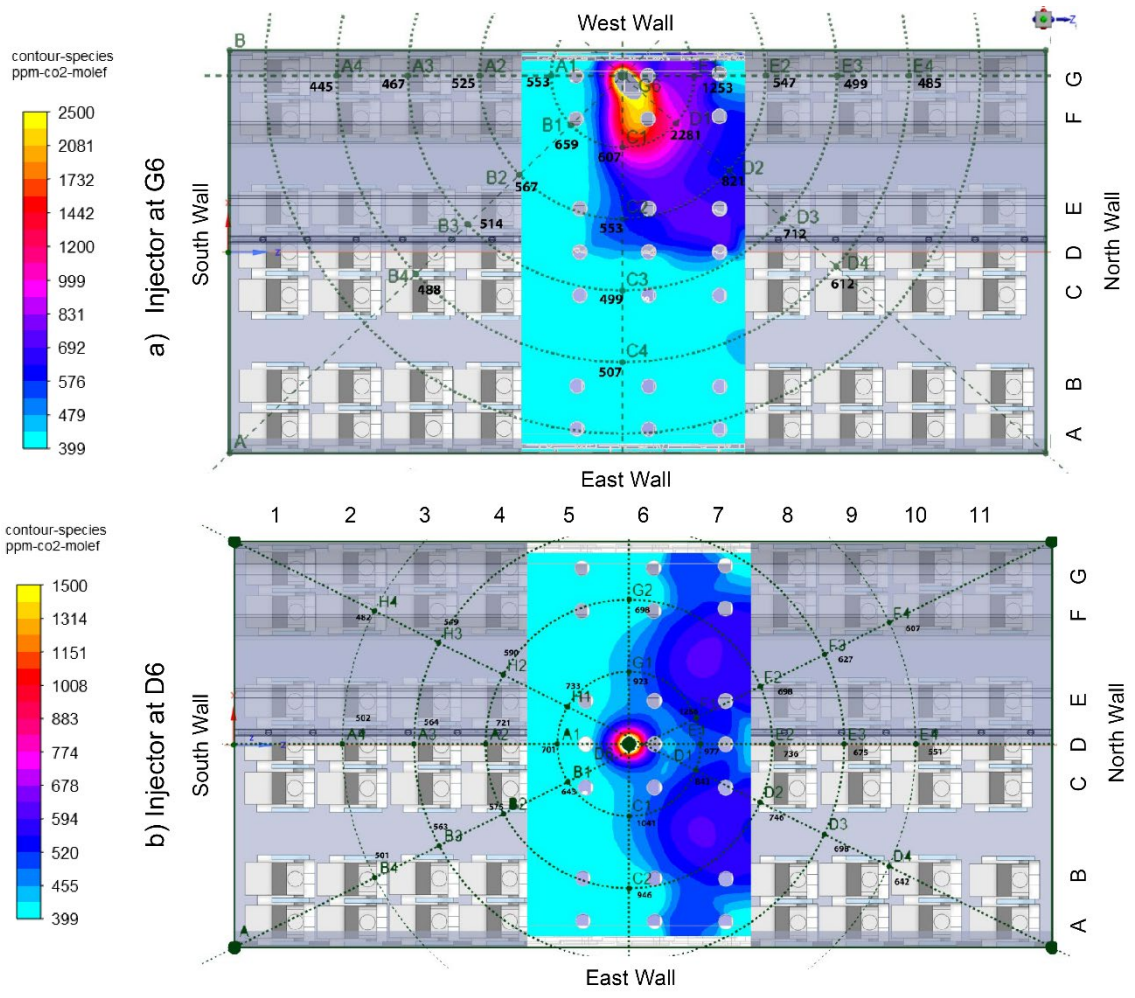

Figure 7. Gaspers off: Comparison of CO_2 molar fractions at breathing area injected at a) side, and b) center.

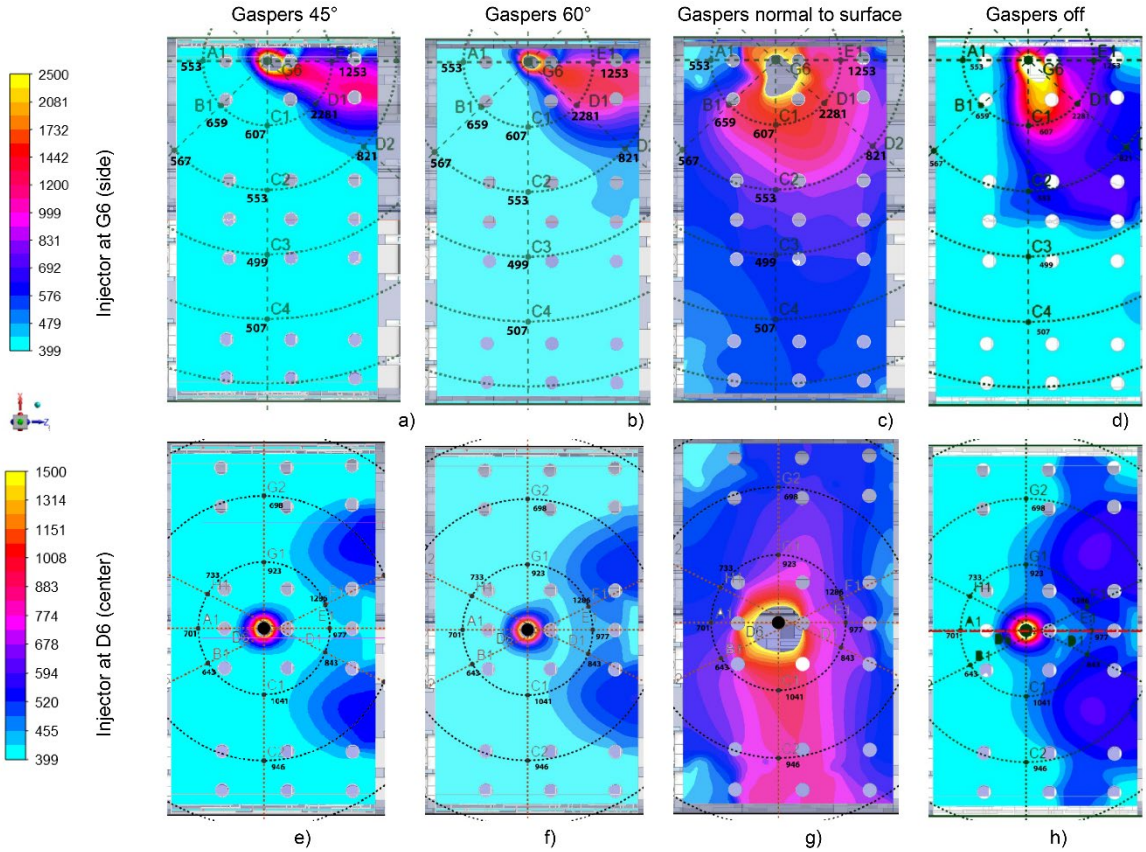

Figure 8. Comparison of CO_2 molar fractions for different gasper settings at the breathing area y = 1.25 m.

With gaspers off, the thermal plumes transfer momentum to the convective transport of the contaminant CO_2. When injected at the side wall, and because of the low ceiling, the contaminant is transported to row 7 eventually putting the passengers in risk. On other hand, when injected at D6, the contaminant climbs higher, which allows it to dissipate into the back rows, storage bins and aisles. Surprisingly, it appears that passengers seating next to the source D6 are not that much affected by the contaminant due to the thermal plumes and the large vortex that pushes the air away [25]. However, when injected at the side, there is significant transverse transport explained by the presence of a small vortex caused by the flow as seen in Figure 6 a).

4.4 Effect of Gaspers

The impact of gaspers on the continuous injection of the tracer gas was studied as well as the variation in velocity direction, using the same mesh (for each inclination), by adjusting the velocity components at the boundary conditions dialog box. The tested velocity inclinations were as follows: normal to the surface where the gaspers were in, at an inclination of 45° and 60° with the *XZ* plane. The gaspers were only tilted across the *YZ* plane.

When the gasper was tilted, there was a significant amount of momentum added to the longitudinal direction which transported the contaminant to the back row, while the vertical velocity was not enough to overcome the buoyancy of the thermal plumes, thus allowing the contaminant to dissipate upwards but closer to the seating passengers. This can be desirable because of the counter-clockwise circulation that will act pushing the contaminant to the storage bin. However, when injected at the side of the cabin, the close proximity to the ceiling remains to be detrimental, thereby increasing the concentration of contaminant at the 7th row.

By analyzing Figure 8 one creates the perception that the gaspers at the baseline experiment were tilted on the side passengers and normal to the surface in the center as shown in b) and g). Finally, when gaspers are normal to the surface, the concentration of CO_2 increases significantly because the upward current caused by thermal plume and the vortex are reduced by the gaspers cold jet. Conjugating these effects, the net result is the decrease of the convection transport which will magnify the diffusion of the contaminant. Further research

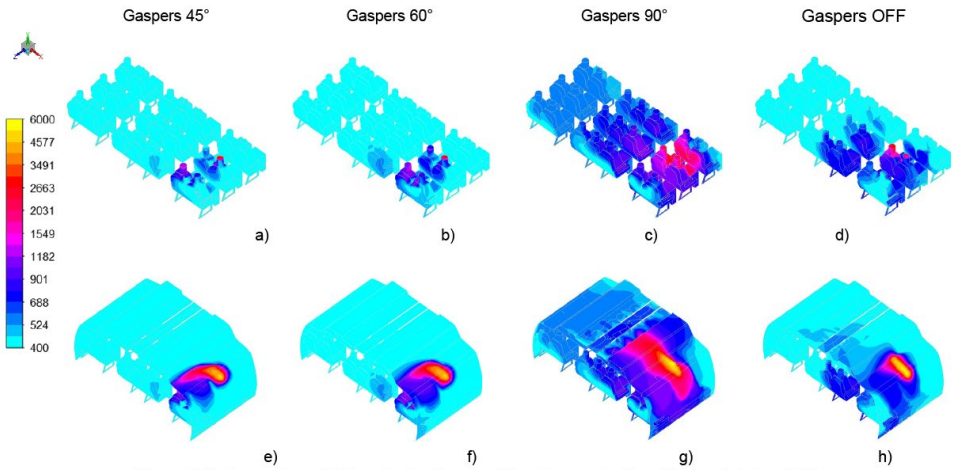

Figure 9. Comparison of CO_2 molar fractions for different gasper settings 3D view, injector at G6.

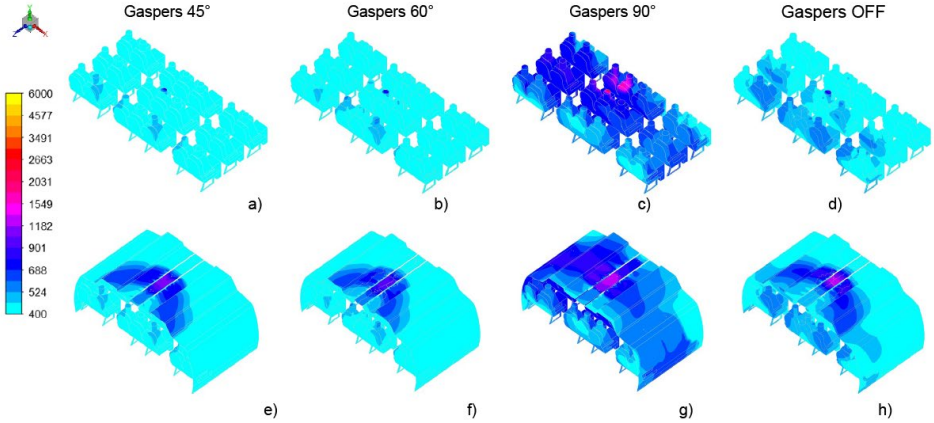

Figure 10 Comparison of CO_2 molar fractions for different gasper settings 3D view, injector at D6

should be carried out to potentially create a protocol to fix the position of gaspers for the safest position.

4.5 Sensors Location

Sensors should be placed at locations with the highest concentration of contaminants. Figure 9 and Figure 10 show the 3D views of the CO_2 molar fractions at the walls in ppm for different gasper settings with injection at G6 and D6, respectively. From a) to d) the displayed surfaces are the walls containing seats and manikins, whereas e) to h) the cabin walls and outlets are overlayed. It can be seen in all figures that the CO_2 is pushed to the ceiling reaching around 5000 ppm when is injected at G6, and around 1000 ppm when injected at D6.

The second possible suitable location is at the backseat of the front seat. In this case, light aerosols would have very low concentration, however, such place might be a good candidate for larger droplets collection.

5. Conclusions

The present work firstly modeled the mockup 767 cabin of KSU using available geometry data.

This allowed to greatly improve the accuracy of the boundary conditions in the aircraft cabin by simulating the complex behavior of the air jets upstream the slot area using a modified RANS realizable k-ε model, which has demonstrated to produce a good agreement with available experimental data.

The model established for the air flow simulation subsequently allowed to also simulate a continuous injection source of a contaminant at the center and at the side of the cabin. In the absence of gaspers, the concentration of the contaminant is higher near the ceiling walls due to the thermal plumes.

When gaspers were added, the inclination of the gasper was crucial for determining the fate of the contaminant. By activating the gaspers normal to the ceilings, the combination of the cold jet with the thermal plume leads to a scenario closer to still air, whereas the longitudinal velocity remained small, thus leading to a decrease in longitudinal spread and increasing diffusion.

When gaspers were tilted to the manikin, there is a significant increase in longitudinal velocity without a major decrease in strength of the thermal plume. Furthermore, turning on gaspers reduced the flow rate available to the supply air. This decreased the strength

of the global designed pattern, thus limiting the control the designer intended.

Using the present models, inspection of wall contamination contours suggest that the best places to install sensors would be on the ceiling right above the passenger, and in the backseat surface of the front seat.

6. Acknowledgements

I would like to thank my supervisor Professor João Melo de Sousa and his constant insightful feedback, motivation, patience as well as sharing knowledge and experience with me.

7. References

[1] ICAO. Effects of Novel Coronavirus (COVID-19) on Civil Aviation: Economic Impact Analysis. *Economic Development* (2022).

[2] IATA. Cabin Air & Low Risk of On Board Transmission.

[3] Raposo, C. L. S. Bioaerosol Transport and Sensor in Passenger Aircraft (MSc. Thesis). (Instituto Superior Técnico, 2022).

[4] Kinahan, S. M., Silcott, D. B., Silcott, B. E., *et al.* Aerosol tracer testing in Boeing 767 and 777 aircraft to simulate exposure potential of infectious aerosol such as SARS-CoV-2. *PLoS One* 1–19 (2021)

[5] Silcott, D. B., Kinahan, S. M., Santarpia, J. L., *et al. TRANSCOM/AMC Commercial Aircraft Cabin Aerosol Dispersion Tests*. (2020).

[6] Davis, A. C., Zee, M., Clark, A. D., *et al.* Computational Fluid Dynamics Modeling of Cough Transport in an Aircraft Cabin. *Sci. Rep.* **11**, (2021)

[7] Shehadi, M. F. Air Quality and Airflow Characteristic Studies for Passenger Aircraft Cabins. In *Indoor Environment and Health* (IntechOpen, 2019).

[8] Mahmoud, S. Experimental Analysis of aerosol dispersion and containment solutions in aircraft cabins (PhD Thesis). (Kansas State University, 2021).

[9] Lin, C.-H., Dunn, K. H., Horstman, R. H., *et al.* Numerical Simulation of Airflow and Airborne Pathogen Transport in Aircraft Cabins - Part I: Numerical Simulation of the Flow Field. *ASHRAE Trans.* **111**, 755–764 (2005)

[10] Lin, C.-H., Horstman, R. H., Ahlers, M. F., *et al.* Numerical Simulation of Airflow and Airborne Pathogen Transport in Aircraft Cabins - Part II: Numerical simulation of Airborne Pathogen Transport. *ASHRAE Trans.* **111**, 764–768 (2005)

[11] Mazumdar, S. Transmission of Airborne Contaminants of Airliner Cabins (PhD Thesis). (Purdue University, 2009).

[12] Isukapalli, S. S., Mazumdar, S., George, P., *et al.* Computational fluid dynamics modeling of transport and deposition of pesticides in an aircraft cabin. *Atmos. Environ.* **68**, 198–207 (2013)

[13] Boeing. *767 Airplane Characteristics for Airport Planning*. *D6-58328* (2012).

[14] Anderson, M. D. Effect of gaspers on airflow patterns and the transmission of airborne contaminants within an aircraft cabin environment (MSc. Thesis). (Kansas State University, 2012).

[15] Shehadi, M. F. Experimental investigation of optimal particulate sensor location in an aircraft cabin (MSc. Thesis). (Kansas State University, 2010).

[16] ANSYS, I. *ANSYS Fluent Theory Guide*. (2021).

[17] Liu, M., Chang, D., Liu, J., *et al.* Experimental investigation of air distribution in an airliner cabin mockup with displacement ventilation. *Build. Environ.* **191**, 107577 (2021)

[18] You, R., Liu, W., Chen, J., *et al.* Predicting airflow distribution and contaminant transport in aircraft cabins with a simplified gasper model. *J. Build. Perform. Simul.* **9**, 699–708 (2016)

[19] National Geodetic Survey. Surface Gravity Prediction. https://geodesy.noaa.gov/cgi-bin/grav_pdx.prl.

[20] Moran, M. J., Shapiro, H. N., Boettner, D. D. & Bailey, M. B. *Fundamentals of Engineering Thermodynamics*. (Wiley, 2018).

[21] CFD Online. Turbulence Intensity. https://www.cfd-online.com/Wiki/Turbulence_intensity.

[22] de Tilly, A. & Sousa, J. M. M. An experimental study of heat transfer in a two-dimensional T-junction operating at a low momentum flux ratio. *Int. J. Heat Mass Transf.* **51**, 941–947 (2008)

[23] Ebrahimi, K., Hosni, M. H. & Zheng, Z. C. Computational Study of Turbulent Airflow in a Full-Scale Aircraft Cabin Mockup - Part 1: Determination of Boundary Conditions at the Outlet of Air Diffusers. In *ASME 2013 Fluids Engineering Division Summer Meeting* vol. 1 A (2013).

[24] Shehadi, M. F., Hosni, M. H. & Jones, B. W. Airflow Distribution in the Longitudinal Plan of a Boeing 767 Mockup Cabin. In *ASME International Mechanical Engineering Congress and Exposition, Proceedings (IMECE)* vol. 7 (2014).

[25] Melo, M. J., Sousa, J. M. M., Costa, M. & Levy, Y. Flow and Combustion Characteristics of a Low-NOx Combustor Model for Gas Turbines. *J. Propuls. Power* **27**, 1212–1217 (2011)